

# On Primordial Black Holes generated from inflation with solo/multi-bumpy potential

Ruifeng Zheng,<sup>1,\*</sup> Jiaming Shi,<sup>1,†</sup> and Taotao Qiu<sup>2,‡</sup>

<sup>1</sup>*Institute of Astrophysics, Central China Normal University, Wuhan 430079, China*

<sup>2</sup>*School of Physics, Huazhong University of Science and Technology, Wuhan, 430074, China*

It is well known that primordial black hole (PBH) can be generated in inflation process of the early universe, especially when the inflaton field has some non-trivial features that could break the slow-roll condition. In this paper, we investigate a toy model of inflation with bumpy potential, which has one or several bumps. We found that potential with multi-bump can give rise to power spectra with multi-peaks in small-scale region, which can in turn predict the generation of primordial black holes in various mass ranges. We also consider the two possibilities of PBH formation by spherical collapse and elliptical collapse.

## I. INTRODUCTION

Since the beginning of the 21st century, the science of astronomy and astrophysics have been developing faster and faster, and people have been paying more and more attention to a kind of evenly mysterious objects: black holes. From 2015 to now, there have been dozens of gravitational wave events coming out, where gravitational wave signals are released from either binary black holes, or other compact objects like white dwarfs and neutron stars [1, 2]. In 2019, the working group of Event Horizon Telescope (EHT) claimed to obtain the first images of the shadow of the supermassive black hole in the center of M87 galaxy [3]. Moreover, the recent (2020) Nobel Prize in Physics was also awarded to studies on the black hole. Along with the development of modern science and technology, it is expected that more information about this object will be discovered by the human beings.

Black holes are classified into many categories, due to different ways. One kind of the black holes attractive to astronomers and cosmologists are called primordial black holes (PBHs) [4, 5]. Unlike astrophysical black holes, PBHs are not formed from the collapse of stars. Instead, they are formed in the primordial universe which is much earlier than the star formation, due to the gravitational collapse by the overdensity of cosmic spacetime in local patches. For this reason, the formed PBHs can have broad mass ranges, which is not constrained by Chandrasekhar and Oppenheimer limits.

In order to form PBHs, one needs small-scale inhomogeneities, and this can be provided by the mechanism of primordial perturbations production during the inflation process in the early universe. In inflation scenario [6–8], where the universe expand to very large extensions within a short time, the quantum fluctuations of the vacuum of the inflaton field will be stretched out of the horizon and become classical perturbations (see, e.g., [9] for a comprehensive review). If the inflation has some feature that makes those perturbations exceed certain threshold value at small scales, then when the perturbations re-enters the horizon, it will cause large inhomogeneities of the universe, and the PBHs will form. There have been long discussions on the formation of PBHs from inflation models, see [10–46]. Among those models, the simplest one are a single field inflation in framework of General Relativity, however, as has been pointed out in [17, 18], slow-roll condition has to be violated in order to form PBHs that consists of all the dark matter. For this reason, slow-roll violating models become an interesting alternative, including ultra-slow-roll inflation [19], inflation with inflection points or bumps [17, 23, 31, 33, 38, 42] and others.

On the other hand, it is well-known that PBHs can work as dark matter, but has been constrained by many experiments, such as Subaru Hyper Suprime-Cam (Subaru-HSC) [47], Experience de Recherche d’Objets Sombres (EROS) [48], Optical Gravitational Lensing Experiment (OGLE) [49], Cosmic Microwave Background (CMB) [50], Femtolensing of Gamma-ray Bursts (FL) [51], White Dwarf Explosions (WD) [52], 511 keV gamma-ray line [53], BH evaporation [54], Neutron Stars (NS) [55], NANOGrav [56], LIGO [57], Leo-I dwarf galaxy [58], Gravitational-Wave Lensing (GW-Lensing) [59] and so on [96]. The upper limits on the PBH fraction of dark matter  $f_{PBH}$  provided by those experiments has nowadays covered almost all over the mass ranges of PBHs, but most of the limits can only reach up to about  $10^{-5}$ , therefore there are still large blank for the PBHs in other mass ranges to have larger fractions. In this paper, we investigate the generalized bumpy inflation model, whose potential contain multiple bumps. For multi-bumpy potential, it is expected that the PBHs can be formed in various mass ranges, therefore comparing to

\*Electronic address: [zrf2021@mails.ccn.u.edu.cn](mailto:zrf2021@mails.ccn.u.edu.cn)

†Co-first author: [2016jimshi@mails.ccn.u.edu.cn](mailto:2016jimshi@mails.ccn.u.edu.cn)

‡Corresponding author: [qiutt@hust.edu.cn](mailto:qiutt@hust.edu.cn)

single mass range, the detectability of the PBHs can get enlarged. If in the future accuracies of these experiments get furtherly improved and the upper limits are put even lower, we can expect that the PBHs generated in our model are more probable to be detected. Note that similar multi-range PBH formation can be realized in [60], with multi-field inflation model.

The rest of our paper is organized as follows: In Sec. II, we show the general formulation of inflation process at both background and perturbation level. For the sake of analyticity, we impose the slow-roll and ultra-slow-roll conditions. In Sec. III, we introduce our inflation models where the inflaton potential has one or multiple bumps (we take the example of 3 bumps), and calculate the slow-roll parameter power spectrum numerically. In Sec. IV, we calculate the fraction of generated PBHs from our models in dark matter, making use of Press-Schechter formalism. We also consider the formation of PBHs in the case of spherical collapse and ellipsoidal collapse. In Sec. V, we come to our conclusions and discussions. Moreover, we take the sign difference to be +2, and the unit where  $c = \hbar = 1$  and  $M_{pl} = 1/\sqrt{8\pi G}$  in this paper.

## II. INFLATION: BASIC FORMULATIONS

We start with the inflation scenario driven by a single scalar field with an arbitrary potential. The action of the inflation model is

$$S = \int d^4x \sqrt{-g} \left[ \frac{M_{pl}^2 R}{2} - \frac{1}{2} \partial_\mu \phi \partial^\mu \phi - V(\phi) \right]. \quad (1)$$

From the above action, we can get the Friedmann equation:

$$H^2 = \frac{1}{3M_{pl}^2} \left( \frac{1}{2} \dot{\phi}^2 + V(\phi) \right), \quad (2)$$

where  $H = \dot{a}/a$  is the Hubble parameter while  $a$  is the scale factor, and dot denotes derivative with respect to cosmic time  $t$ . We can also get the equation of motion of the inflaton field  $\phi$ :

$$\ddot{\phi} + 3H\dot{\phi} + V'(\phi) = 0, \quad (3)$$

where  $V'(\phi) = dV(\phi)/d\phi$ . In order to maintain inflation process, it is usually required that the slow-roll condition should be obeyed. We define the slow-roll parameters as follows:

$$\epsilon_H = -\frac{\dot{H}}{H^2}, \quad (4)$$

$$\eta_H = -\frac{\ddot{H}}{2\dot{H}H}, \quad (5)$$

$$\xi_H = \frac{\dddot{H}}{2H^2\dot{H}} - 2\eta_H^2, \quad (6)$$

where the subscript  $H$  denotes that these parameters are defined for the Hubble parameter, or in other words, the “whole universe”. The slow-roll condition states that during inflation all these parameters have the values much smaller than 1, namely

$$|\epsilon_H|, |\eta_H|, |\xi_H| \ll 1. \quad (7)$$

On the other hand, one can also define another set of slow roll parameters using the inflaton potential itself:

$$\epsilon_V = \frac{M_{pl}^2}{2} \left( \frac{V'(\phi)}{V(\phi)} \right)^2, \quad (8)$$

$$\eta_V = M_{pl}^2 \frac{V''(\phi)}{V(\phi)}, \quad (9)$$

and when the slow-roll condition (7) holds, one has  $\epsilon_H \simeq \epsilon_V$ ,  $\eta_H \simeq \eta_V - \epsilon_V$ . Moreover, we usually use the total number of e-foldings to describe the duration of inflation:

$$N \equiv N_i - N_e = \int_{t_i}^{t_e} H(t) dt = \ln \left( \frac{a_e}{a_i} \right). \quad (10)$$

where the subscript  $i$  and  $e$  denotes parameters at the beginning and ending time of inflation, respectively. In order to solve the notorious Big-Bang problems, it is usually required that  $N \geq 60$  [61].

Now we turn to the perturbations generated during inflation. The perturbed FRW metric in its 3+1 decomposed form is [62]:

$$ds^2 = a^2(\tau)[-(1 + 2\alpha)d\tau^2 + 2\partial_i\beta d\tau dx^i + e^{h_{ij} + 2\zeta\delta_{ij}} dx^i dx^j], \quad (11)$$

where  $\alpha$ ,  $\beta$ ,  $\zeta$  are the scalar-type perturbations, and  $h_{ij}$  is the tensor-type perturbation. The comoving time  $\tau$  is defined by the relation  $d\tau \equiv a^{-1}(t)dt$ . In uniform- $\phi$  gauge,  $\alpha$  and  $\beta$  become constraint degrees of freedom only, and the only dynamical scalar perturbation is  $\zeta$  [63, 64]. In order to get an analytical solution of  $\zeta$ , we define the well-known Mukhanov-Sasaki (MS) variable  $u$  as:

$$u \equiv z\zeta, \quad z \equiv a \frac{\dot{\phi}}{H}, \quad (12)$$

and this variable satisfies Mukhanov-Sasaki equation in the Fourier space as [65, 66]:

$$u_k'' + \left(k^2 - \frac{z''}{z}\right) u_k = 0, \quad (13)$$

where prime denotes derivative with respect to comoving time  $\tau$ , and the effective potential term is given by the following expression:

$$\frac{z''}{z} = 2a^2 H^2 \left(1 + \epsilon_H - \frac{3}{2}\eta_H + \epsilon_H^2 + \frac{1}{2}\eta_H^2 - 2\epsilon_H\eta_H + \frac{1}{2}\xi_H\right). \quad (14)$$

For a given mode  $k$ , for sub-Hubble region with  $k \gg aH$  at sufficiently early times, we can assume  $u_k$  to be quantum fluctuations in the Bunch-Davies vacuum [67] satisfying

$$u_k(\tau) \rightarrow \frac{1}{\sqrt{2k}} e^{-ik\tau}. \quad (15)$$

The above solution can be viewed as the initial condition of the MS variable  $u_k$ . However, as the inflation process will lead to the decline of comoving Hubble radius, the  $k$ -mode will exit the horizon and enter the super-Hubble region with  $k \ll aH$ , while the quantum fluctuations will decoherent and become classical perturbations. By solving the MS equation and making use of the relation between the MS variable and its dimensionless primordial power-spectrum [14]

$$P_S = \frac{k^3}{2\pi^2} \frac{|u_k|^2}{z^2} \Big|_{k \ll aH}, \quad (16)$$

we obtain the power spectrum expression under the slow roll approximation:

$$P_S = \frac{1}{8\pi^2 \epsilon_H} \left(\frac{H}{M_{pl}}\right)^2. \quad (17)$$

On the large cosmological scale accessible to CMB observations, the power spectrum usually takes the power-law form:

$$P_R(k) = A_S \left(\frac{k}{k_*}\right)^{n_s - 1} \quad (18)$$

where  $A_S = P_S(k_*)$  is the amplitude of the scalar power spectrum at the pivot scale. In the slow-roll approximation, the scalar spectral tilt  $n_s$  are given by [61]

$$n_s = 2\eta_H - 4\epsilon_H + 1. \quad (19)$$

Recent CMB observations suggest  $P_S \simeq 2.1 \times 10^{-9}$  at  $k_* = 0.05 \text{Mpc}^{-1}$  [68], while in order to increase the abundance of PBH to an appropriate order of magnitude,  $P_S$  must reach the amount of  $O(10^{-2})$ . Note that when slow-roll condition holds,  $P_S$  will be conserved in time and will not deviate too much from its pivot value, therefore it is

impossible to generate enough PBHs, and we must break the condition. This is also pointed out in recent papers such as [17, 18]. One way is to have  $\epsilon_H$  decrease rapidly at small scales, while keep the results at large scales unchanged. One of such a model is the ultra-slow-roll (USR) inflation model [69–71]. In this model, one has absolute flat potential, therefore

$$\ddot{\phi} + 3H\dot{\phi} = -V'(\phi) = 0, \quad \epsilon_H \propto a^{-6}. \quad (20)$$

Therefore  $\epsilon_H$  get decreased with the explosion of  $a$ , leading to a sharp increase in  $P_S$  according to Eq.(17) [19]. Moreover, in this case, the slow-roll condition gets violated because  $\eta_H = 3 + \epsilon_H > 1$ , and the above relations between two sets of the slow-roll parameters do not hold any longer. Another example is the featured potential like the one with a bump [38, 42]. When the inflaton passes through the bump, it will enter a state similar to USR, which will achieve a local enhancement of the power spectrum.

### III. OUR MODELS

#### A. solo-bumpy potential

In this subsection, we construct inflaton field with one bump in its potential. We take the potential to be of the following form:

$$V(\phi) = V_0 \left( \frac{\phi}{M_{pl}} \right)^p \left( 1 + b e^{-\frac{(\phi-c)^2}{d}} \right). \quad (21)$$

Here the basic potential is of power-law form while there is Gaussian function-like bump on the potential. The parameters  $b$ ,  $c$  and  $d$  denotes the height, the central value in  $\phi$  and the width of the bump. From this potential, one gets

$$\epsilon_V = \frac{M_{pl}^2}{2} \frac{\left( p d e^{\frac{(c-\phi)^2}{d}} + b (p d + 2(c-\phi)\phi) \right)^2}{d^2 \left( b + e^{\frac{(c-\phi)^2}{d}} \right)^2 \phi^2}, \quad (22)$$

$$\eta_V = M_{pl}^2 \left( \frac{p(p-1)}{\phi^2} - \frac{2b\phi(\phi d + 2p\phi d + 4c\phi^2 - 2\phi^3 - 2cpd - 2c^2\phi)}{\phi^2 \left( b + e^{\frac{(c-\phi)^2}{d}} \right) d^2} \right). \quad (23)$$

In Fig. 1, we plot various relations between variables involved in this case. In the numerical calculation, we choose the parameters as:

$$V_0 = 1.45 \times 10^{-11} M_{pl}^4, \quad p = 2, \quad b = 1.5718 \times 10^{-2}, \quad c = 11 M_{pl}, \quad d = 5 \times 10^{-3} M_{pl}^2. \quad (24)$$

From the plot, we can easily see that there is a bump in the potential at  $\phi = 11 M_{pl}$ . Due to the bump, the inflaton will stay around  $\phi = 11 M_{pl}$  for a short while. However, if the initial velocity of  $\phi$  is insufficient, inflaton may stop at the bump forever and can not continue to roll, leading to an eternal inflation. On the other hand, if the initial velocity of the inflaton is too large, the inflaton will pass through the bump very quickly, which will make the peak value of the power spectrum too low to have enough abundance of the PBHs. Therefore, both the initial velocity and the parameters of the bump need to be carefully settled. In the numerical calculation, we set the initial value of  $\phi$  to be  $\phi_i = 16.2 M_{pl}$ , from which  $\phi$  rolls down, and the initial velocity of  $\phi$  to be  $\dot{\phi}_i = 4.5 \times 10^{-6}$ , so as to satisfy the observational constraint from CMB.

We solve equation of motion (3) for scalar field  $\phi$  to obtain its evolution with respect to e-folding number  $N$ . From the plot we can see that the inflaton meet the bump near  $N = 40$ . We also plot the evolution of  $\epsilon_H$  and  $\eta_H$  with respect to  $N$ . In order to increase the power spectrum amplitude to  $10^{-2}$ , the inflaton will stay at the bump for about 7 e-folding numbers. Because of the very slow motion of the inflaton, the slow roll parameter  $\epsilon_H$  gets very small value, while  $\eta_H$  becomes very large ( $\sim O(1)$ ), just like the case of USR inflation models. Moreover, the inflation can stop when  $\epsilon = 1$  around  $N = 70$ .

We also solve the MS equation (13) numerically and get the variation of the power spectrum  $P_S$  with respect to the wave number  $k$ . We can see that the power spectrum fits the constraints from CMB on large scales while have a peak value of  $O(10^{-2})$  (the numerical value is 0.02284) at  $k = 1 \times 10^{14} \text{ Mpc}^{-1}$ .

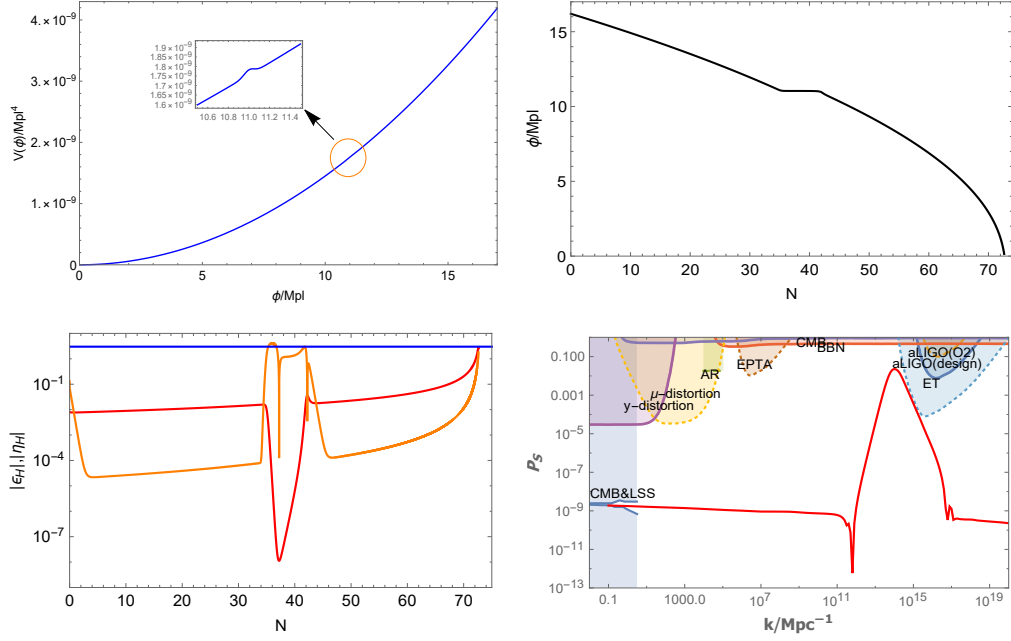


FIG. 1: *The upper left figure:* the inflation potential of  $p = 2$ , and the bump is located at  $\phi = 11M_{pl}$ . *The upper right figure:* the evolution of  $\phi$  with the parameter  $N$ , which enters the USR-like stage near  $N = 40$ . *The lower left figure:* the evolution of the slow roll parameters  $|\epsilon_H|$  and  $|\eta_H|$ , and the blue line corresponds to the value of 3 on the vertical axis. *The lower right figure:* the relationship between power spectrum  $P_S$  (in Logarithmic scale) and the wave-number  $k$ . Our results are consistent with the observational constraints.

For a further verification, we choose a second set of parameters as

$$V_0 = 4.96 \times 10^{-10} M_{pl}^4, \quad p = 2/3, \quad b = 5.9921 \times 10^{-3}, \quad c = 6M_{pl}, \quad d = 2 \times 10^{-3} M_{pl}^2. \quad (25)$$

and plot the same figures in Fig. 2. We see that in this case, the decrease of  $\epsilon_H$  happens around  $N = 20$  during inflation and we will have a peak in power spectrum at around  $k = 1 \times 10^6 Mpc^{-1}$ . Therefore, we find that the Gaussian-function-like bump on the potential does lead to the peak on the spectrum at small scales, as long as we correctly choose the parameters. Such a feature in the spectrum can in principle generate PBHs, which we will discuss in the next section.

## B. multi-bumpy potential

In this subsection, we extend the model discussed above to the case where the potential have more than one bump. In this case, there will be multiple peaks in the power spectrum, leading to formation of PBHs in multiple mass ranges. It is interesting in the sense that, in the future when the accuracy of the experiments are getting higher and higher, it is expected that PBHs can be caught in various mass ranges, which can thus be explained by our model. In the following, we take the potential to be of the following form:

$$V(\phi) = V_0 \left( \frac{\phi}{M_{pl}} \right)^2 \left( 1 + b_1 e^{-\frac{(\phi-c_1)^2}{d_1}} + b_2 e^{-\frac{(\phi-c_2)^2}{d_2}} + b_3 e^{-\frac{(\phi-c_3)^2}{d_3}} + \dots \right). \quad (26)$$

In principle, there could be arbitrary numbers of bumps in the potential, however, we in this paper take an example of three Gaussian function-like bumps for the sake of simplicity and analyticity. The specific parameters of Eq.(26) are given as

$$\begin{aligned} b_1 &= 1.571806 \times 10^{-2}, \quad c_1 = 11M_{pl}, \quad d_1 = 5 \times 10^{-3} M_{pl}^2, \\ b_2 &= 1.41793 \times 10^{-2}, \quad c_2 = 12M_{pl}, \quad d_2 = 5 \times 10^{-3} M_{pl}^2, \\ b_3 &= 1.29364 \times 10^{-2}, \quad c_3 = 13M_{pl}, \quad d_3 = 5 \times 10^{-3} M_{pl}^2. \end{aligned} \quad (27)$$

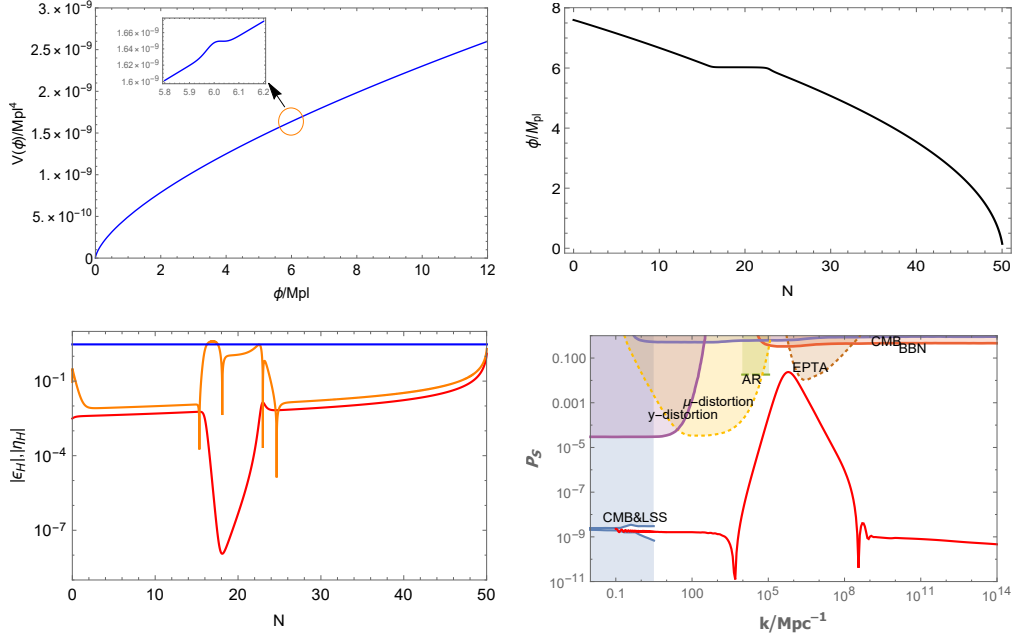


FIG. 2: The upper left figure: the inflation potential of  $p = 2/3$ , and the bump is located at  $\phi = 6M_{pl}$ . The upper right figure: the evolution of  $\phi$  with the parameter  $N$ , which enters the USR-like stage near  $N = 20$ . The lower left figure: the evolution of the slow roll parameters  $|\epsilon_H|$  and  $|\eta_H|$ , and the blue line corresponds to the value of 3 on the vertical axis. The lower right figure: the relationship between power spectrum  $P_S$  (in Logarithmic scale) and the wave-number  $k$ . Our results are consistent with the observational constraints.

In this case, the inflaton rolls down from the value of  $\phi = 16.2M_{pl}$  satisfies the observation constraint of CMB from Fig. 3. We set  $V_0 = 1.45 \times 10^{-11} M_{pl}^4$ .

It is easy to see that there are three USR stages in the Fig. 3, which means that there will be three peaks in the power spectrum. For initial conditions, we still set  $\phi_i = 16.2M_{pl}$  and  $\dot{\phi}_i = 4.5 \times 10^{-6}$ , the same as for the solo-bumpy model. However, different from the solo-bumpy ones, we have to take care of not only the shape of each bump (height, width, etc), but also the relative distance of the bumps. This is important because, when the inflaton field passes through one bump, it will lose kinetic energy, and if the bumps are far from each other, it may not have enough energy to pass through the next ones. For this reason, in this paper we set the bumps close to each other, namely at  $\phi = 11M_{pl}$ ,  $\phi = 12M_{pl}$  and  $\phi = 13M_{pl}$ . We can see from the plot that we will have three times that  $\eta_H$  breaks the slow-roll condition around  $N = 20$ ,  $N = 35$  and  $N = 50$ , leading to three peaks on the power spectrum in small scales, while the inflation finally ends at around  $N = 87$ , while both  $\epsilon_H$  and  $\eta_H$  exceeds unity. As will be shown in the next section, this will form PBHs in three different mass ranges.

#### IV. PBH FORMATION AND ABUNDANCE

We first briefly review how the PBHs are formed from inflation and how to relate the mass of PBHs to inflation power spectrum. Roughly speaking, if the fluctuations re-entering the horizon becomes large enough, the primordial black holes with extensive mass will form due to gravitational collapse. The mass of PBHs formed at a certain epoch in the radiation dominated era with fluctuation mode  $k_{PBH}$  is given by the Hubble mass at that epoch up to an efficiency factor  $\gamma$  [72, 73]:

$$M_{PBH} = \gamma M_H = \gamma \frac{4\pi}{3} H_{form}^{-3} \rho_{form} , \quad (28)$$

where when the PBHs were formed, the Hubble radius and the energy density of the universe are denoted by  $H_{form}^{-1}$  and  $\rho_{form}$  respectively, and  $M_H$  is the total mass inside the Hubble radius. Moreover, in radiation dominated era, we have  $\gamma \simeq 0.2$ . With the Friedmann equation:  $3H_{form}^2 = 8\pi G \rho_{form}$ , Eq. (28) can be written in another form:

$$M_{PBH} = \gamma \sqrt{\frac{2\pi}{3G}} \rho_{form}^{1/2} H_{form}^{-2} . \quad (29)$$

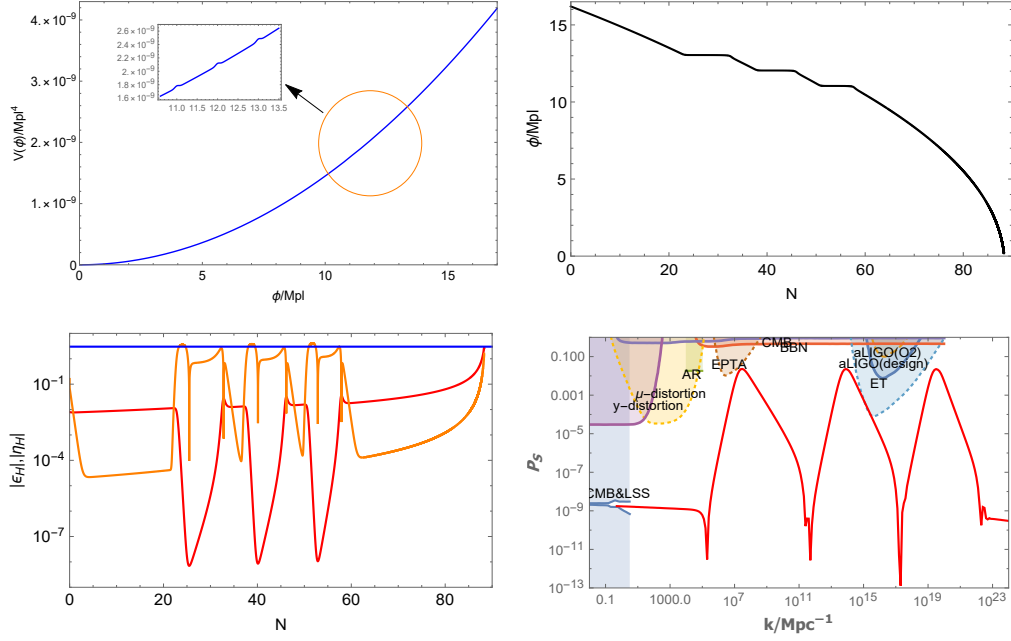


FIG. 3: The upper left figure: the inflation potential with three bumps locating at  $\phi = 11\text{Mpl}$ ,  $\phi = 12\text{Mpl}$  and  $\phi = 13\text{Mpl}$ . The upper right figure: the evolution of  $\phi$  with the parameter  $N$ , which enters the USR-like stage three times near  $N = 20$ ,  $N = 35$  and  $N = 50$ . The lower left figure: the evolution of the slow roll parameters  $|\epsilon_H|$  and  $|\eta_H|$ , and the blue line corresponds to the value of 3 on the vertical axis. The lower right figure: the relationship between power spectrum  $P_s$  (in Logarithmic scale) and the wave-number  $k$ . Our results are consistent with the observational constraints.

Note that in radiation dominated era,  $\rho = \frac{\pi^2}{30}g_*T^4$ , and in the adiabatic environment of the early universe, entropy density:  $s \sim g_*T^3 \sim a^{-3}$ , therefore  $T \sim g_*^{-1/3}a^{-1}$  [74]. Then we can get [75]

$$\begin{aligned}
 M_{PBH} &= \gamma \sqrt{\frac{2\pi}{3G}} \left( \frac{g_*}{g_{*eq}} \right)^{1/2} \left( \frac{T_{form}}{T_{eq}} \right)^2 \left( \frac{H_{form}}{H_{eq}} \right)^{-2} \rho_{eq}^{1/2} H_{eq}^{-2} \\
 &= \gamma \sqrt{\frac{2\pi}{3G}} \left( \frac{g_*}{g_{*eq}} \right)^{1/2} \left( \frac{g_*}{g_{*eq}} \right)^{-2/3} \left( \frac{a_{form}}{a_{eq}} \right)^{-2} \left( \frac{H_{form}}{H_{eq}} \right)^{-2} \rho_{eq}^{1/2} H_{eq}^{-2} \\
 &= \gamma \frac{1}{2G} H_{eq}^{-1} \left( \frac{g_*}{g_{*eq}} \right)^{-1/6} \left( \frac{k_{form}}{k_{eq}} \right)^{-2} \\
 &= 2 \times 10^{48} g \times \left( \frac{\gamma}{0.2} \right) \left( \frac{g_*}{106.75} \right)^{-1/6} \left( \frac{k_{form}}{0.07 \text{ Mpc}^{-1}} \right)^{-2}, \tag{30}
 \end{aligned}$$

where  $g_*$  is the total effective degree of freedom of the universe in the radiation dominated era. The subscript “form” denotes variables that are evaluated when PBHs were formed, and the subscript “eq” denotes variables that are evaluated when radiation and matter are equal to each other. Note that in the radiation/matter equality,  $g_{*eq} \simeq 3.38$  and  $k_{eq} \simeq 0.07 \Omega_{m0} h^2 \text{Mpc}^{-1}$ . We can thus see that, the mass of PBHs are determined by the scale of its formation denoted by  $k_{form}$ . For a given  $k_{form}$ , we can get the corresponding  $M_{PBH}$ .

We are interested in whether the PBHs formed can act as dark matter, or more precisely, how much fraction of dark matter can be contributed from the PBHs. To evaluate this, we need to define the fraction of PBHs in dark matter, namely

$$f_{PBH} = \frac{\rho_{PBH}}{\rho_{DM}} \bigg|_{form}, \tag{31}$$

and this can be connected to the fraction of PBHs in the whole universe

$$\beta(M_{PBH}) \equiv \frac{\rho_{PBH}}{\rho_{tot}} \bigg|_{form}, \tag{32}$$

via the equation:

$$\begin{aligned} f_{PBH} &= \beta(M_{PBH}) \left( \frac{\rho_{tot}}{\rho_{DM}} \right) \Big|_{form} \\ &= \beta(M_{PBH}) \Omega_{DM0}^{-1} \left( \frac{a_0}{a_{form}} \right)^{-3} \left( \frac{H_{form}}{H_0} \right)^2, \end{aligned} \quad (33)$$

where subscript “0” denotes variables evaluated today, and  $\Omega_{DM0}$  is the today’s density fraction of dark matter that can be obtained from the observations. Combining Eqs. (30) and (33) and doing some manipulations (the details of which could be found in, e.g. [54]), we can get the relationship between  $\beta(M)$  and  $f_{PBH}$ :

$$f_{PBH}(M_{PBH}) = 1.68 \times 10^8 \left( \frac{\gamma}{0.2} \right)^{1/2} \left( \frac{g_*}{106.75} \right)^{-1/4} \left( \frac{M_{PBH}}{M_\odot} \right)^{-1/2} \beta(M_{PBH}). \quad (34)$$

The standard treatment of  $\beta(M)$  is based on the Press-Schechter formalism [76] of the gravitational collapse that is used widely in large-scale structure studies [77]. In this formalism,  $\beta(M)$  is given by the probability that the fractional overdensity  $\delta \equiv \delta\rho/\rho$  is above a certain threshold  $\delta_c$  for PBH formation [78, 79]. For Gaussian primordial fluctuations,  $\beta(M)$  is given by [80, 81]:

$$\begin{aligned} \beta(M(k)) &= 2 \int_{\delta_c}^{\infty} \exp\left(-\frac{\delta^2}{2\sigma^2(M(k))}\right) \frac{d\delta}{\sqrt{2\pi}\sigma(M(k))} \\ &= \sqrt{\frac{2}{\pi}} \frac{\sigma(M(k))}{\delta_c} \exp\left(-\frac{\delta_c^2}{2\sigma^2(M(k))}\right), \end{aligned} \quad (35)$$

As can be seen from the above formula, the value of the  $\beta(M)$  is uniquely determined by the variance  $\sigma^2(M(k))$  which is assumed to be coarse-grained variance smoothed on a scale of  $R = k^{-1}$ . During the radiation dominated era, it is given by the following expression [82]:

$$\sigma^2(M(k)) = \frac{16}{81} \int_0^\infty d\ln q \left( \frac{q}{k} \right)^4 W\left( \frac{q}{k} \right)^2 P_S^2(q), \quad (36)$$

where  $P_S^2(q)$  is the power spectrum of curvature perturbation and  $W(x)$  is smoothing window function [83, 84]. In this paper, we use Gaussian form:  $W(x) = \exp(-x^2/2)$ . Moreover, In general, in the radiation dominated period, the threshold density  $\delta_c = c_s^2 = 1/3 \approx 0.33$ . However, some studies have shown that the threshold density  $\delta_c$  can be between 0.33 and 0.66 [85, 86].

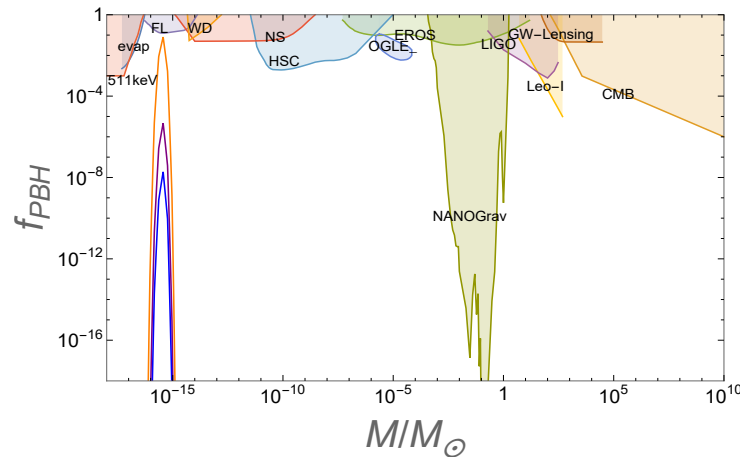


FIG. 4: We plot  $f_{PBH}$  for potential (21) with  $p = 2$  using different threshold densities  $\delta_c$ , where the yellow line corresponds to  $\delta_c = 0.41$ , the purple line corresponds to  $\delta_c = 0.46$ , and the blue line corresponds to  $\delta_c = 0.486$ . Our results are consistent with the constraints from current observations [87]. The specific parameters are shown in Table I. Constraints are obtained from the publicly available **Python** code **PBHbounds** [88].

| $k_{form}/Mpc^{-1}$     | $M_{PBH}$                      | $\delta_c$ | $f_{PBH}$               |
|-------------------------|--------------------------------|------------|-------------------------|
| $1.1539 \times 10^{14}$ | $3.68 \times 10^{-16} M_\odot$ | 0.41       | $8.0455 \times 10^{-2}$ |
| $1.1539 \times 10^{14}$ | $3.68 \times 10^{-16} M_\odot$ | 0.46       | $4.6573 \times 10^{-6}$ |
| $1.1539 \times 10^{14}$ | $3.68 \times 10^{-16} M_\odot$ | 0.486      | $1.8905 \times 10^{-8}$ |

TABLE I:  $f_{PBH}$  for potential (21) with  $p = 2$  for different threshold densities  $\delta_c$ .

| $k_{form}/Mpc^{-1}$     | $M_{PBH}$                      | $\delta_c$ | $f_{PBH}$               | $f_{e-PBH}$             |
|-------------------------|--------------------------------|------------|-------------------------|-------------------------|
| $1.1539 \times 10^{14}$ | $3.68 \times 10^{-16} M_\odot$ | 0.41       | $8.0455 \times 10^{-2}$ | $1.1781 \times 10^{-8}$ |

TABLE II:  $f_{PBH}$  and  $f_{e-PBH}$  for potential (21) with  $p = 2$  and  $\delta_c = 0.41$ .

In Fig. 4, we numerically plot the abundances of  $f_{PBH}$  with different threshold energy  $\delta_c$ , taking solo-bumpy potential with  $p = 2$  as an example. Values of  $\delta_c$  as in Table I. We find that the larger  $\delta_c$  is, the smaller the abundance will be, and this is easy understanding: the larger the threshold energy is, the more difficult it is to form black holes. For the small value of  $\delta_c = 0.41$ , the abundance of PBHs can reach around 10% of dark matter. The mass range of the PBHs formed is around  $10^{-15} M_\odot$ , namely the asteroid mass.

Moreover, we also considered the case where the PBHs formed in the early universe was ellipsoidal collapse instead of spherical collapse [89, 90]. The difference between these two collapse models is that the threshold density for forming PBH is different. Because compared with the spherical collapse, the PBHs formed by the ellipsoidal collapse will increase the ellipticity of the formed PBHs, which will lead to the correction of the threshold density. In the following, we uniformly use PBHs/e-PBHs to represent the primordial black hole formed by spherical collapse/ellipsoidal collapse, and  $\delta_c/\delta_{ec}$  to describe the threshold density of PBHs/e-PBHs, respectively. According to [91, 92] we have the following relation:

$$\delta_{ec} = \delta_c \left[ 1 + \kappa \left( \frac{\sigma^2}{\delta_c^2} \right)^\nu \right], \quad (37)$$

where  $\kappa = 9/\sqrt{10\pi}$  and  $\nu = 1/2$ . From Eq. (34), we can easily obtain the abundance of PBHs and e-PBHs with a given  $\delta_c$ . The calculation shows that the abundance of e-PBHs is lower than that of PBHs, due to the difference in their threshold densities.

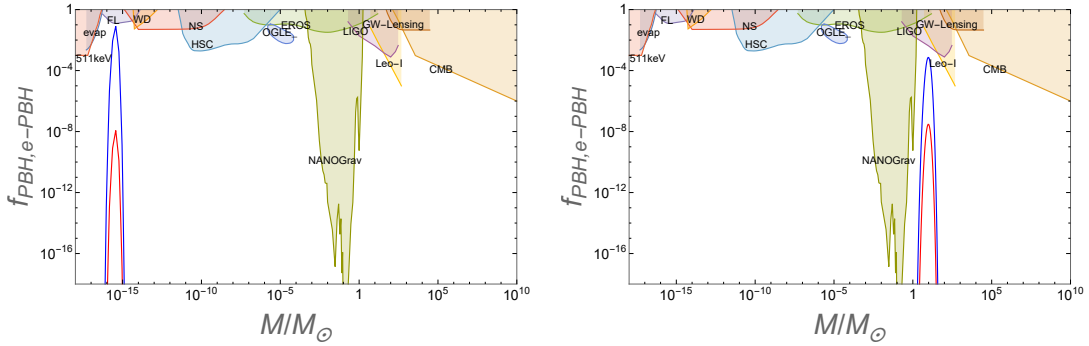


FIG. 5: The figures above show the constraints on primordial black holes acting as dark matter, in which the colored region is excluded by various observations. The blue line correspond to  $f_{PBH}$ , and the red line correspond to  $f_{e-PBH}$ . The left figure is for potential (21) with  $p = 2$  and  $\delta_c = 0.41$ , while the right figure is for potential (21) with  $p = 2/3$  and  $\delta_c = 0.33$ . Constraints are obtained from the publicly available **Python** code **PBHbounds** [88].

In Fig. 5, We plot the abundances of  $f_{PBH}$  and  $f_{e-PBH}$  from solo-bumpy potential (21), with parameter sets  $\{p = 2, \delta_c = 0.41\}$  and  $\{p = 2/3, \delta_c = 0.33\}$  respectively, as well as constraints from various observations. For  $p = 2$  case, the fraction of PBHs could reach  $O(10\%)$  at the mass range of  $\sim 10^{-15} M_\odot$  (asteroid mass), while for  $p = 2/3$  case, the fraction is also nearly  $O(0.1\%)$  at the mass range of  $\sim 1 M_\odot$  (solar mass). The specific parameters are shown in Table. II and Table. III.

Similarly, we plot the abundances of  $f_{PBH}$  and  $f_{e-PBH}$  from multi-bumpy potential (26) (with parameter sets (27)) in Fig. 6. As can be seen from the figure, PBHs can be formed in three mass ranges. The leftmost peak in

| $k_{form}/Mpc^{-1}$  | $M_{PBH}$        | $\delta_c$ | $f_{PBH}$               | $f_{e-PBH}$             |
|----------------------|------------------|------------|-------------------------|-------------------------|
| $6.0256 \times 10^5$ | $9.2437 M_\odot$ | 0.33       | $7.2256 \times 10^{-4}$ | $2.9602 \times 10^{-8}$ |

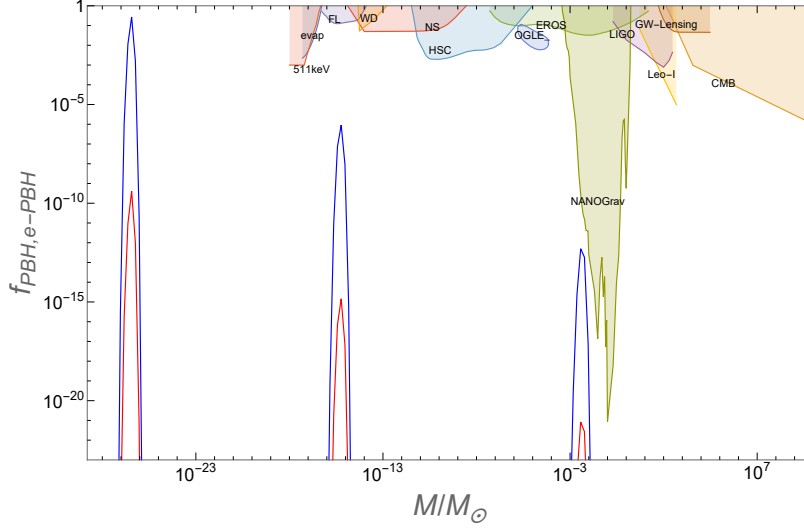
TABLE III:  $f_{PBH}$  and  $f_{e-PBH}$  for potential (21) with  $p = 2/3$  and  $\delta_c = 0.33$ .

FIG. 6: The figures above show the constraints on primordial black holes acting as dark matter, in which the colored region is excluded by various observations. The blue line correspond to  $f_{PBH}$ , and the red line correspond to  $f_{e-PBH}$ . The plot is for potential (26) and  $\delta_c = 0.465$ . From left to right, the masses of PBHs are  $3.6975 \times 10^{-27} M_\odot$ ,  $5.8601 \times 10^{-16} M_\odot$  and  $3.6975 \times 10^{-3} M_\odot$  respectively. Constraints are obtained from the publicly available **Python** code **PBHbounds** [88].

Fig. 6 we can have large amount of PBHs, the abundance of which can reach 27% of dark matter, however, since the mass range of PBHs is too small (around  $3.6975 \times 10^{-27} M_\odot$ ), if one considers effects of Hawking radiation, such PBHs may not have chance to live till today. Nonetheless, it may have some non-trivial effects in the evolution of the Universe, which we will mention in the next section. On the other hand, the other two peaks refer to PBHs of  $10^{-15} M_\odot$  (asteroid mass) and  $10^{-3} M_\odot$  (planet mass), which can live till today and may act as dark matter. The specific values are shown in Table. IV.

## V. CONCLUSION

In this paper, we investigate the formation of PBHs from inflation model with bumpy features on its potential. Although the case of potential with one bump has been discussed in the literature, we discuss the extended case of multiple bumps, which can generate PBHs at different mass ranges. This will enlarge the detectability of PBHs from the coming development of the astronomical observations. Specifically, we take the power-law potential as the basic potential, and add one or several bumps of Gaussian type which makes the inflaton roll from the slow-roll stage to USR-like stage. With the potential, we construct the power spectrum with single or multiple peaks in small scales, while keeping the large scale power spectrum consistent with CMB data. We numerically calculate the abundances of PBHs (fraction to dark matter) at the mass range given by the solo-bumpy potential, as well as three mass ranges given by the multi-bumpy potential. Thanks to those peaks, PBHs can be formed at different mass ranges, including asteroid mass range ( $10^{-16} - 10^{-14} M_\odot$ ), planet mass range ( $10^{-6} - 10^{-3} M_\odot$ ) and solar mass range (around  $1 M_\odot$ ),

| $k_{form}/Mpc^{-1}$     | $M_{PBH}$                        | $\delta_c$ | $f_{PBH}$                | $f_{e-PBH}$              |
|-------------------------|----------------------------------|------------|--------------------------|--------------------------|
| $3.1548 \times 10^{19}$ | $3.6975 \times 10^{-27} M_\odot$ | 0.465      | $2.7181 \times 10^{-1}$  | $4.0947 \times 10^{-10}$ |
| $7.9245 \times 10^{13}$ | $5.8601 \times 10^{-16} M_\odot$ | 0.465      | $9.0930 \times 10^{-7}$  | $1.4448 \times 10^{-15}$ |
| $3.1548 \times 10^7$    | $3.6975 \times 10^{-3} M_\odot$  | 0.465      | $4.9587 \times 10^{-13}$ | $8.3559 \times 10^{-22}$ |

TABLE IV:  $f_{PBH}$  and  $f_{e-PBH}$  for potential (26) and  $\delta_c = 0.465$ .

some of which can reach significant abundance. We also show that the abundance has a negative correlation with the threshold energy density  $\delta_c$ . We confront the results to the current observational data, and all the abundances are consistent with the data constraints. Although we take three bumps for simplicity, in principle from such kind of potential, abundances at other mass ranges are also expected.

Moreover, PBHs formed in the early universe may also be formed by ellipsoidal collapse. Therefore, we not only considered the formation of spherical collapsed PBHs, but also considered the formation of PBHs under ellipsoidal collapse, due to the correction brought by the ellipticity of the latter, thus according to the Press-Schechter formalism, the abundance will be lower. We obtain the abundances of PBHs in the two types of collapse at all the mass ranges discussed above, and find the numerical result consistent with the analytical analysis.

Before ending, let's briefly mention about the evaporation of the formed PBHs. According to Hawking's theory of black hole radiation, these black holes will inevitably emit virtual particles and cause their mass smaller and smaller till vanishing, which is known as Hawking evaporation [93]. It has been pointed out that, considering the age of the universe, PBHs with initial mass less than  $10^{15}\text{g}$  ( $\sim 10^{-18}M_\odot$ ) has been completely evaporated today. Therefore for the multi-bumpy inflation model in our analysis, the PBHs standing for the leftmost peak in FIG. 6 will actually be vanishing, and cannot explain the dark matter today. However, it does not mean that they are not important at all. Actually, they may still have a significant impact on the early universe, such as the process of Big Bang Nucleosynthesis, reheating, baryogenesis and so on [93–95]. With the further development of observational techniques, we may be able to detect the traces left by the PBHs of this type, to find more evidence of their existence. Meanwhile, for other mass ranges, the PBHs are hardly evaporated till now and thus can act as dark matter. The more details about the influences of the PBHs in our model on those other aspects of our universe, although very interesting, are postponed to an upcoming paper.

### Acknowledgments

T. Q. thanks Yun-Gui Gong and Shi Pi for useful discussions. This work was supported by the National Natural Science Foundation of China under Grants No. 11653002 and No. 11875141. J.S. was partially supported by the Fundamental Research Funds for the Central Universities (Innovation Funded Projects) under Grants No. 2020CXZZ105.

- 
- [1] B. P. Abbott *et al.* (LIGO Scientific, Virgo), *Phys. Rev. Lett.* **116**, 061102 (2016), [arXiv:1602.03837 \[gr-qc\]](#) .
  - [2] B. P. Abbott *et al.* (LIGO Scientific, Virgo), *Phys. Rev. Lett.* **119**, 161101 (2017), [arXiv:1710.05832 \[gr-qc\]](#) .
  - [3] K. Akiyama *et al.* (Event Horizon Telescope), *Astrophys. J. Lett.* **875**, L1 (2019), [arXiv:1906.11238 \[astro-ph.GA\]](#) .
  - [4] S. Hawking, *Mon. Not. Roy. Astron. Soc.* **152**, 75 (1971).
  - [5] B. J. Carr and S. W. Hawking, *Mon. Not. Roy. Astron. Soc.* **168**, 399 (1974).
  - [6] A. H. Guth, *Phys. Rev. D* **23**, 347 (1981).
  - [7] A. D. Linde, *Phys. Lett. B* **108**, 389 (1982).
  - [8] A. A. Starobinsky, *Phys. Lett. B* **91**, 99 (1980).
  - [9] A. Riotto, *ICTP Lect. Notes Ser.* **14**, 317 (2003), [arXiv:hep-ph/0210162](#) .
  - [10] J. Garcia-Bellido, A. D. Linde, and D. Wands, *Phys. Rev. D* **54**, 6040 (1996), [arXiv:astro-ph/9605094](#) .
  - [11] M. Drees and E. Erfani, *JCAP* **01**, 035 (2012), [arXiv:1110.6052 \[astro-ph.CO\]](#) .
  - [12] J. Garcia-Bellido and E. Ruiz Morales, *Phys. Dark Univ.* **18**, 47 (2017), [arXiv:1702.03901 \[astro-ph.CO\]](#) .
  - [13] V. Domcke, F. Muia, M. Pieroni, and L. T. Witkowski, *JCAP* **07**, 048 (2017), [arXiv:1704.03464 \[astro-ph.CO\]](#) .
  - [14] G. Ballesteros and M. Taoso, *Phys. Rev. D* **97**, 023501 (2018), [arXiv:1709.05565 \[hep-ph\]](#) .
  - [15] K. Kannike, L. Marzola, M. Raidal, and H. Veermäe, *JCAP* **09**, 020 (2017), [arXiv:1705.06225 \[astro-ph.CO\]](#) .

- [16] B. Carr, T. Tenkanen, and V. Vaskonen, *Phys. Rev. D* **96**, 063507 (2017), arXiv:1706.03746 [astro-ph.CO] .
- [17] C. Germani and T. Prokopec, *Phys. Dark Univ.* **18**, 6 (2017), arXiv:1706.04226 [astro-ph.CO] .
- [18] H. Motohashi and W. Hu, *Phys. Rev. D* **96**, 063503 (2017), arXiv:1706.06784 [astro-ph.CO] .
- [19] H. Di and Y. Gong, *JCAP* **07**, 007 (2018), arXiv:1707.09578 [astro-ph.CO] .
- [20] O. Özsoy, S. Parameswaran, G. Tasinato, and I. Zavala, *JCAP* **07**, 005 (2018), arXiv:1803.07626 [hep-th] .
- [21] M. Biagetti, G. Franciolini, A. Kehagias, and A. Riotto, *JCAP* **07**, 032 (2018), arXiv:1804.07124 [astro-ph.CO] .
- [22] Y.-F. Cai, X. Tong, D.-G. Wang, and S.-F. Yan, *Phys. Rev. Lett.* **121**, 081306 (2018), arXiv:1805.03639 [astro-ph.CO] .
- [23] T.-J. Gao and Z.-K. Guo, *Phys. Rev. D* **98**, 063526 (2018), arXiv:1806.09320 [hep-ph] .
- [24] R.-g. Cai, S. Pi, and M. Sasaki, *Phys. Rev. Lett.* **122**, 201101 (2019), arXiv:1810.11000 [astro-ph.CO] .
- [25] G. Ballesteros, J. Beltran Jimenez, and M. Pieroni, *JCAP* **06**, 016 (2019), arXiv:1811.03065 [astro-ph.CO] .
- [26] C. T. Byrnes, P. S. Cole, and S. P. Patil, *JCAP* **06**, 028 (2019), arXiv:1811.11158 [astro-ph.CO] .
- [27] I. Dalianis, *JCAP* **08**, 032 (2019), arXiv:1812.09807 [astro-ph.CO] .
- [28] S. Pi, M. Sasaki, and Y.-l. Zhang, *JCAP* **06**, 049 (2019), arXiv:1904.06304 [gr-qc] .
- [29] S. A. Vallejo-Peña and A. E. Romano, *JCAP* **11**, 015 (2019), arXiv:1904.07503 [astro-ph.CO] .
- [30] I. Dalianis and G. Tringas, *Phys. Rev. D* **100**, 083512 (2019), arXiv:1905.01741 [astro-ph.CO] .
- [31] N. Bhaumik and R. K. Jain, *JCAP* **01**, 037 (2020), arXiv:1907.04125 [astro-ph.CO] .
- [32] C. Fu, P. Wu, and H. Yu, *Phys. Rev. D* **100**, 063532 (2019), arXiv:1907.05042 [astro-ph.CO] .
- [33] W.-T. Xu, J. Liu, T.-J. Gao, and Z.-K. Guo, *Phys. Rev. D* **101**, 023505 (2020), arXiv:1907.05213 [astro-ph.CO] .
- [34] J. Liu, Z.-K. Guo, and R.-G. Cai, *Phys. Rev. D* **101**, 023513 (2020), arXiv:1908.02662 [astro-ph.CO] .
- [35] C. Chen and Y.-F. Cai, *JCAP* **10**, 068 (2019), arXiv:1908.03942 [astro-ph.CO] .
- [36] R. Arya, *JCAP* **09**, 042 (2020), arXiv:1910.05238 [astro-ph.CO] .
- [37] R. Mahbub, *Phys. Rev. D* **101**, 023533 (2020), arXiv:1910.10602 [astro-ph.CO] .
- [38] S. S. Mishra and V. Sahni, *JCAP* **04**, 007 (2020), arXiv:1911.00057 [gr-qc] .
- [39] J. Lin, Q. Gao, Y. Gong, Y. Lu, C. Zhang, and F. Zhang, *Phys. Rev. D* **101**, 103515 (2020), arXiv:2001.05909 [gr-qc] .
- [40] C. Fu, P. Wu, and H. Yu, *Phys. Rev. D* **102**, 043527 (2020), arXiv:2006.03768 [astro-ph.CO] .
- [41] G. Ballesteros, J. Rey, M. Taoso, and A. Urbano, *JCAP* **08**, 043 (2020), arXiv:2006.14597 [astro-ph.CO] .
- [42] O. Özsoy and Z. Lalak, *JCAP* **01**, 040 (2021), arXiv:2008.07549 [astro-ph.CO] .
- [43] M. Solbi and K. Karami, (2021), arXiv:2102.05651 [astro-ph.CO] .
- [44] K.-Y. Choi, S.-b. Kang, and R. N. Raveendran, (2021), arXiv:2102.02461 [astro-ph.CO] .
- [45] Q. Gao, (2021), arXiv:2102.07369 [gr-qc] .
- [46] K. Inomata, E. McDonough, and W. Hu, (2021), arXiv:2104.03972 [astro-ph.CO] .
- [47] H. Niikura *et al.*, *Nature Astron.* **3**, 524 (2019), arXiv:1701.02151 [astro-ph.CO] .
- [48] P. Tisserand *et al.* (EROS-2), *Astron. Astrophys.* **469**, 387 (2007), arXiv:astro-ph/0607207 .

- [49] H. Niikura, M. Takada, S. Yokoyama, T. Sumi, and S. Masaki, *Phys. Rev. D* **99**, 083503 (2019), [arXiv:1901.07120 \[astro-ph.CO\]](#) .
- [50] Y. Ali-Haïmoud and M. Kamionkowski, *Phys. Rev. D* **95**, 043534 (2017), [arXiv:1612.05644 \[astro-ph.CO\]](#) .
- [51] A. Barnacka, J. F. Glicenstein, and R. Moderski, *Phys. Rev. D* **86**, 043001 (2012), [arXiv:1204.2056 \[astro-ph.CO\]](#) .
- [52] P. W. Graham, S. Rajendran, and J. Varela, *Phys. Rev. D* **92**, 063007 (2015), [arXiv:1505.04444 \[hep-ph\]](#) .
- [53] R. Laha, *Phys. Rev. Lett.* **123**, 251101 (2019), [arXiv:1906.09994 \[astro-ph.HE\]](#) .
- [54] B. J. Carr, K. Kohri, Y. Sendouda, and J. Yokoyama, *Phys. Rev. D* **81**, 104019 (2010), [arXiv:0912.5297 \[astro-ph.CO\]](#) .
- [55] F. Capela, M. Pshirkov, and P. Tinyakov, *Phys. Rev. D* **87**, 123524 (2013), [arXiv:1301.4984 \[astro-ph.CO\]](#) .
- [56] Z.-C. Chen, C. Yuan, and Q.-G. Huang, *Phys. Rev. Lett.* **124**, 251101 (2020), [arXiv:1910.12239 \[astro-ph.CO\]](#) .
- [57] B. J. Kavanagh, D. Gaggero, and G. Bertone, *Phys. Rev. D* **98**, 023536 (2018), [arXiv:1805.09034 \[astro-ph.CO\]](#) .
- [58] B.-Q. Lu and Y.-L. Wu, *Phys. Rev. D* **99**, 123023 (2019), [arXiv:1906.10463 \[astro-ph.HE\]](#) .
- [59] S. Jung and C. S. Shin, *Phys. Rev. Lett.* **122**, 041103 (2019), [arXiv:1712.01396 \[astro-ph.CO\]](#) .
- [60] Y. Tada and S. Yokoyama, *Phys. Rev. D* **100**, 023537 (2019), [arXiv:1904.10298 \[astro-ph.CO\]](#) .
- [61] D. Baumann, in *Theoretical Advanced Study Institute in Elementary Particle Physics: Physics of the Large and the Small* (2009) [arXiv:0907.5424 \[hep-th\]](#) .
- [62] R. L. Arnowitt, S. Deser, and C. W. Misner, *Gen. Rel. Grav.* **40**, 1997 (2008), [arXiv:gr-qc/0405109](#) .
- [63] J. M. Maldacena, *JHEP* **05**, 013 (2003), [arXiv:astro-ph/0210603](#) .
- [64] X. Chen, M.-x. Huang, S. Kachru, and G. Shiu, *JCAP* **01**, 002 (2007), [arXiv:hep-th/0605045](#) .
- [65] M. Sasaki, *Prog. Theor. Phys.* **76**, 1036 (1986).
- [66] V. F. Mukhanov, *Sov. Phys. JETP* **67**, 1297 (1988).
- [67] T. S. Bunch and P. C. W. Davies, *Proc. Roy. Soc. Lond. A* **360**, 117 (1978).
- [68] Y. Akrami *et al.* (Planck), *Astron. Astrophys.* **641**, A10 (2020), [arXiv:1807.06211 \[astro-ph.CO\]](#) .
- [69] W. H. Kinney, *Phys. Rev. D* **72**, 023515 (2005), [arXiv:gr-qc/0503017](#) .
- [70] M. H. Namjoo, H. Firouzjahi, and M. Sasaki, *EPL* **101**, 39001 (2013), [arXiv:1210.3692 \[astro-ph.CO\]](#) .
- [71] J. Martin, H. Motohashi, and T. Suyama, *Phys. Rev. D* **87**, 023514 (2013), [arXiv:1211.0083 \[astro-ph.CO\]](#) .
- [72] M. Sasaki, T. Suyama, T. Tanaka, and S. Yokoyama, *Class. Quant. Grav.* **35**, 063001 (2018), [arXiv:1801.05235 \[astro-ph.CO\]](#) .
- [73] A. M. Green and A. R. Liddle, *Phys. Rev. D* **56**, 6166 (1997), [arXiv:astro-ph/9704251](#) .
- [74] E. W. Kolb and M. S. Turner, *The Early Universe*, Vol. 69 (1990).
- [75] K. Inomata, M. Kawasaki, K. Mukaida, Y. Tada, and T. T. Yanagida, *Phys. Rev. D* **96**, 043504 (2017), [arXiv:1701.02544 \[astro-ph.CO\]](#) .
- [76] W. H. Press and P. Schechter, *Astrophys. J.* **187**, 425 (1974).
- [77] J. Sureda, J. Magana, I. J. Araya, and N. D. Padilla, (2020), [arXiv:2008.09683 \[astro-ph.CO\]](#) .
- [78] Y.-P. Wu, *Phys. Dark Univ.* **30**, 100654 (2020), [arXiv:2005.00441 \[astro-ph.CO\]](#) .
- [79] R. Mahbub, *Phys. Rev. D* **102**, 023538 (2020), [arXiv:2005.03618 \[astro-ph.CO\]](#) .

- [80] K. Inomata, M. Kawasaki, K. Mukaida, Y. Tada, and T. T. Yanagida, *Phys. Rev. D* **96**, 123527 (2017), [arXiv:1709.07865 \[astro-ph.CO\]](#) .
- [81] B. J. Carr, *Astrophys. J.* **201**, 1 (1975).
- [82] D. Blais, T. Bringmann, C. Kiefer, and D. Polarski, *Phys. Rev. D* **67**, 024024 (2003), [arXiv:astro-ph/0206262](#) .
- [83] K. Tokeshi, K. Inomata, and J. Yokoyama, *JCAP* **12**, 038 (2020), [arXiv:2005.07153 \[astro-ph.CO\]](#) .
- [84] S. Young, *Int. J. Mod. Phys. D* **29**, 2030002 (2019), [arXiv:1905.01230 \[astro-ph.CO\]](#) .
- [85] I. Musco, V. De Luca, G. Franciolini, and A. Riotto, (2020), [arXiv:2011.03014 \[astro-ph.CO\]](#) .
- [86] G. Sato-Polito, E. D. Kovetz, and M. Kamionkowski, *Phys. Rev. D* **100**, 063521 (2019), [arXiv:1904.10971 \[astro-ph.CO\]](#) .
- [87] A. Siraj and A. Loeb, (2021), [arXiv:2104.07672 \[astro-ph.CO\]](#) .
- [88] B. J. Kavanagh, “[bradkav/pbhbounds: Release version,](#)” (2019).
- [89] A. Arbey, J. Auffinger, and J. Silk, in *40th International Conference on High Energy Physics* (2020) [arXiv:2012.14767 \[astro-ph.CO\]](#) .
- [90] M. Mirbabayi, A. Gruzinov, and J. Noreña, *JCAP* **03**, 017 (2020), [arXiv:1901.05963 \[astro-ph.CO\]](#) .
- [91] F. Kühnel and M. Sandstad, *Phys. Rev. D* **94**, 063514 (2016), [arXiv:1602.04815 \[astro-ph.CO\]](#) .
- [92] R. K. Sheth, H. J. Mo, and G. Tormen, *Mon. Not. Roy. Astron. Soc.* **323**, 1 (2001), [arXiv:astro-ph/9907024](#) .
- [93] S. W. Hawking, *Nature* **248**, 30 (1974).
- [94] B. J. Carr, *Astrophys. J.* **206**, 8 (1976).
- [95] D. Baumann, P. J. Steinhardt, and N. Turok, (2007), [arXiv:hep-th/0703250](#) .
- [96] The information of the constraints, along with the references, are obtained from the publicly available **Python** code **PBHbounds** [88].